IL NUOVO CIMENTO VOL. 20 C, N. 5 Settembre-Ottobre 1997

Numerical simulations of X-ray binary pulse profiles(*)

L. BURDERI(1), G. A. WYNN(2) and N. R. ROBBA(3)

(1) *Astronomy Group, University of Leicester - Leicester LE1 7RH, UK*
Istituto di Fisica, Università di Palermo - Palermo, Italy
(2) *Astronomy Group, University of Leicester - Leicester LE1 7RH, UK*
(3) *Istituto di Fisica, Università di Palermo - Palermo, Italy*

(ricevuto il 4 Aprile 1996; approvato il 24 Maggio 1996)

Summary. — We investigate the physical features of the accretion process in magnetic X-ray binaries. The characteristics of the accretion column and the geometrical modulation effects due to the neutron star spin determine the shape of the pulse profile. In order to constrain the possible scenarios, we produce numerical simulations of the X-ray pulse profile, in different energy bands. As an example we reproduce the pulse profile and hardness ratio curve of X Persei. Fan emission from a hollow section of cone, along with a non-thermal component can reproduce the observed data of this source.

PACS 96.40 – Cosmic rays.
PACS 01.30.Cc – Conference proceedings.

1. – Introduction

Pulse profiles, averaged over many periods, are available for all the presently known X-ray pulsars. These profiles are produced over a range of X-ray energies. It is commonly believed that the pulse shapes are determined primarily by emission and absorption processes, as well as geometrical shadowing, within the magnetosphere of a rotating neutron star (NS), that is accreting material from its binary companion. This implies that it is possible to use the X-ray pulse profiles to probe the structure of the magnetosphere, and the plasma conditions during the last stages of the accretion process. The magnetic field of the NS plays a crucial role in the dynamics of the accreting matter and in the production of X-rays. Under a large number of different physical conditions the plasma is threaded by the magnetic field, at least in the last phase of the accretion process. In such cases a stable field-aligned flow is possible only if the kinetic energy density of the plasma is less than the energy density of the magnetic field, *i.e.* $\rho v_{\parallel}^2 < B^2/4\pi$, where $v_{\parallel}$ is the flow velocity parallel to the magnetic field B. The Alfvén radius is defined as the radius at

(*) Paper presented at the VII Cosmic Physics National Conference, Rimini, October 26-28, 1994.

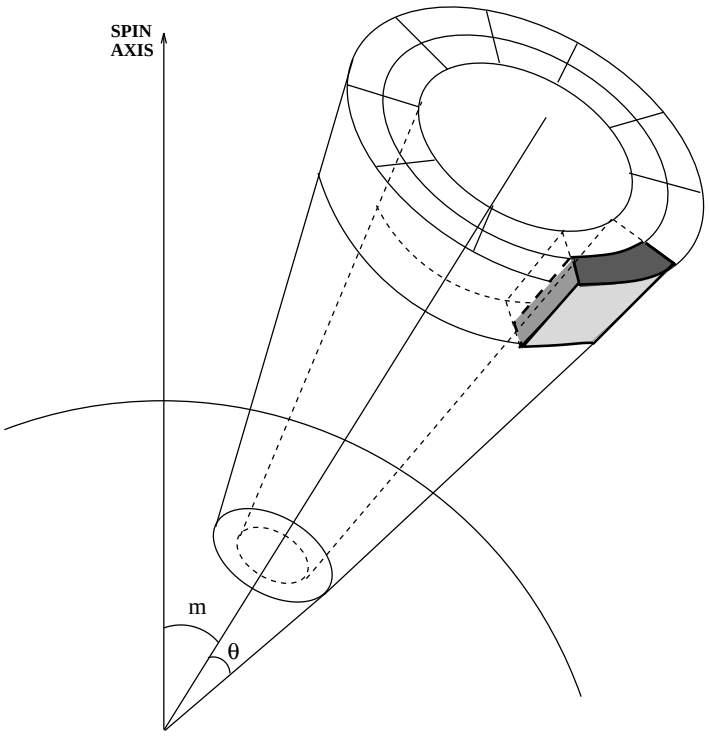

Fig. 1. – Schematic representation of the emission region subdivided into bricks.

which the two energies are equal. Inside this radius the plasma is forced to flow along the magnetic-field lines towards the polar caps, where it is accreted by the NS. In this situation the accreting material forms a column-shaped structure above each magnetic pole. The detailed structure and size of this column, and the radiative processes operating in the plasma determine the (energy dependent) shape of the pulse profile, provided that all the geometrical effects due to the inclination of the magnetic axis and the line of sight with respect to the spin axis are taken into account. In order to investigate this, we have developed a simulation program to produce pulse profiles for different geometrical shapes of the accretion column. This is achieved by dividing the emission region into a number of bricks, each being characterised by its emission function and absorption coefficient. Only the principal emission processes are taken in account. The contribution of the bricks during a rotation of the NS around its spin axis is calculated in order to build up the pulse profile.

2. – The X-ray emission region

The accretion column has been investigated by several authors (*e.g.*, Lamb *et al.* 1973; Basko and Sunyaev 1975; Arons and Lea 1980; Wang and Frank 1981; Wang and Welter 1982; Mészáros *et al.* 1983; White *et al.* 1983), under different assumptions. Some general results, utilised in the simulation code, are summarized below:

- The general shape of the X-ray emission region is that of a section of cone with the apex at the NS centre. The cone geometry is an approximation of the dipole field

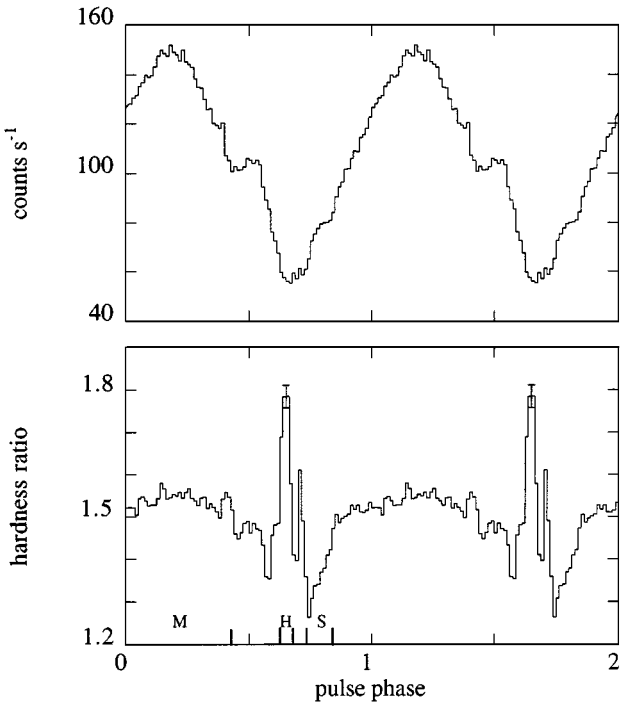

Fig. 2. – Upper panel: time-averaged background-subtracted pulse profile in the 1.5–11.5 keV energy band. Lower panel: hardness ratio curve in the energy band (4–11.5 keV)/(1.5–4 keV).

structure close to the NS surface, which funnels the accretion flow down to the polar caps. The central region of this cone can be free of matter: in the case of accretion via a disc the magnetic-field lines thread the disc material over a restricted region, the result being that the innermost ring of the disc flows along the field lines produces a hollow-cone structure above each polar cap. Even in the case of spherically symmetric accretion from a stellar wind the accretion column can be empty inside, since the first stages of accretion through the magnetosphere proceed via the free fall of diamagnetic blobs generated by Rayleigh-Taylor instabilities, and the magnetospheric regions close to the poles are the most stable to these instabilities.

- The gravitational potential energy of the in-falling plasma is radiated away mainly by means of thermal, and synchrotron emission. The free fall (or spiral-in for disc accretion) of the accreting matter is halted at the magnetosphere. The matter penetrates the magnetosphere via instabilities, and is threaded by the field at the Alfén radius, from which point the matter flows towards the polar caps. The structure of the emission region is dependent on the luminosity of the source. If the luminosity is $\ll L_{\mathrm{Edd}}$, the Eddington luminosity, say $< 10^{37}\ \mathrm{erg\,s^{-1}}$ the column height is dependent on the stopping mechanism of the plasma.

  If it is stopped by Coulomb collisions, the column height Δz is $\ll R_{\mathrm{NS}}$, the radius of the NS. Here we have blackbody-like emission at a temperature $\sim 10^7$ K, and synchrotron radiation. In this case the synchrotron radiation, due to the presence of the strong magnetic field ($\sim 10^{12}$ G) near the NS crust, is important all along the column structure. The synchrotron self-absorption is so high that this emission is

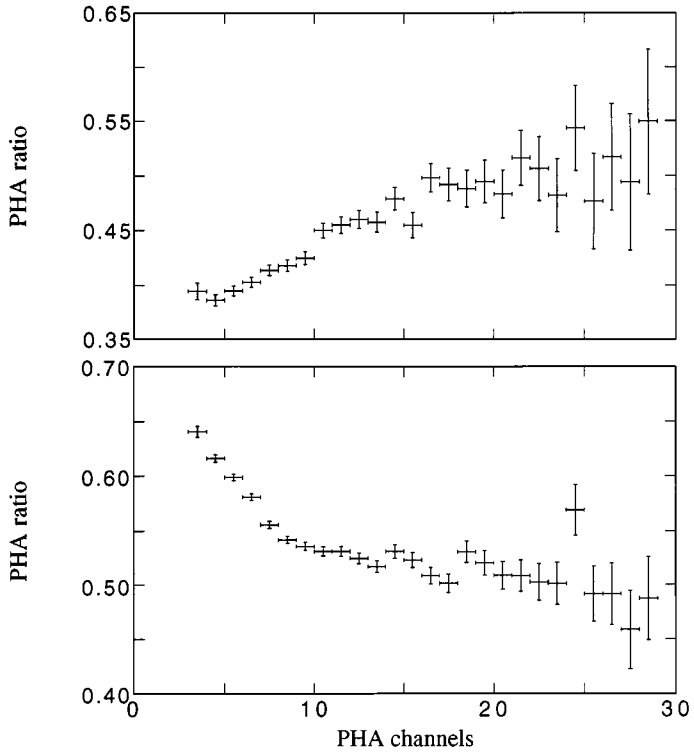

Fig. 3. – Upper panel: ratio of average spectra recorded during phase intervals H and M. Lower panel: same as upper panel using phase intervals S and M. (Phase intervals H, S, and M are defined in fig. 2.)

blackbody-like at the synchrotron frequency ($h\nu \sim 12$ keV B_{12}, where B_{12} is the field in units of 10^{12} G).

If the plasma is stopped via a collisionless shock, the height of the accretion column could be $\gtrsim R_{\rm NS}$. In this case the main emission processes are bremsstrahlung and synchrotron. The bremsstrahlung is emitted throughout the cone at a temperature $\sim 10^7$ K. The synchrotron emission dominates in a ring at the base of the accretion funnel, since the intensity of the synchrotron emission varies as $B^2 \propto r^{-6}$.

If the luminosity is $\gtrsim L_{\rm Edd}$, the radiation pressure can stop the in-falling matter and we can have $\Delta z \sim R_{\rm NS}$. In this case the emission is due to blackbody ($T \sim 10^7$ K), and synchrotron radiation from a mound of slowly settling high-density material at the base of the column, inflated by the radiation pressure.

- The Compton scattering is strongly dependent on the geometrical shape of the emission region $\tau_{\rm c} \sim \sigma_{\rm c} \rho d / m_{\rm p}$, where $\tau_{\rm c}$ is the Compton optical depth, $\sigma_{\rm c}$ is the magnetically reduced Compton cross-section, ρ is the density of the plasma, d is the geometrical path inside the emission region, and $m_{\rm p}$ is the proton mass. In the case of a cone of height Δz and diameter D, we can define $\bar{\tau}_{\|}$ and $\bar{\tau}_{\perp}$, adopting an average density $\bar{\rho}$, as the optical depths parallel and perpendicular to the cone walls. Due to magnetic effects, $\bar{\tau}_{\|}$ is strongly reduced for photon energies below the synchrotron frequency, as $\sigma_{\|} \sim \sigma_{\rm T}(\nu/\nu_{\rm c})^2$, where $\sigma_{\rm T}$ is the Thompson cross-section and $\nu_{\rm c} \propto r^{-3}$ is the

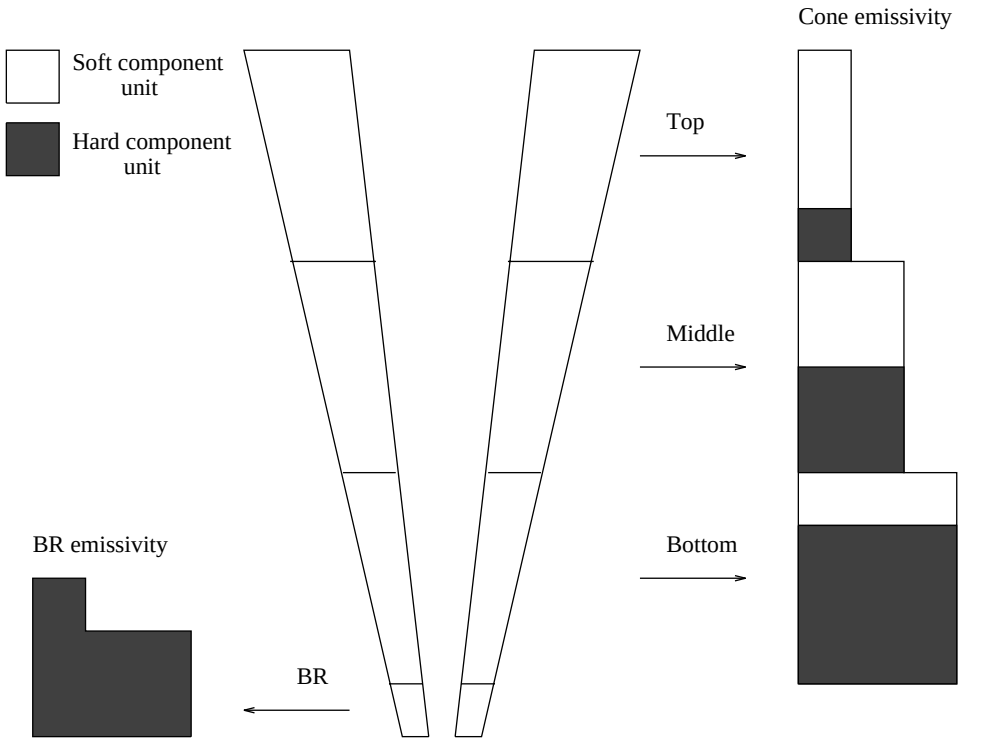

Fig. 4. – Schematic representation of the spatial distribution of the cone emission in terms of hard and soft components.

synchrotron frequency. So in the case of a short cone magnetic reduction is important throughout and we have $\bar{\tau}_{\parallel} < \bar{\tau}_{\perp}$, *i.e.* the radiation is mainly emitted along the magnetic axis: pencil emission. For an extended column, the magnetic reduction becomes unimportant with increasing Δz and we have $\bar{\tau}_{\parallel} > \bar{\tau}_{\perp}$ since $\Delta z > D$. In this case the radiation is mainly emitted perpendicular to the cone axis: fan emission.

Taking all of these effects into account we can schematically describe the geometry of the emission region as a section of hollow cone (sometimes filled at the centre). The emission mechanism along the cone is thermal bremsstrahlung ($\propto \rho^2 T^{1/2}$), the Compton scattering along the cone ($\tau_{\mathrm{c}} = \int \sigma_{\mathrm{c}} \rho d / m_{\mathrm{p}} \, \mathrm{d}x$), determines the character of the source, as being "fan" or "pencil" emission. An optically thick blackbody-like emitting ring or slab is present at the base of the cone, the energy of which depends on whether thermal or synchrotron processes dominate.

3. – Simulating the pulse profiles

The detailed physical processes operating in the accretion column are very complex and, as yet, not completely understood. In particular, the extreme physical conditions and the high intensity of the magnetic field ($\sim 10^{12}\,\mathrm{G}$) near the NS crust make the problem difficult to treat. Moreover, the physics of collisionless shocks is unclear. As a consequence, no self-consistent solutions for an accretion column exist. However, interesting qualitative results can be obtained assuming the density and temperature profiles along the emission

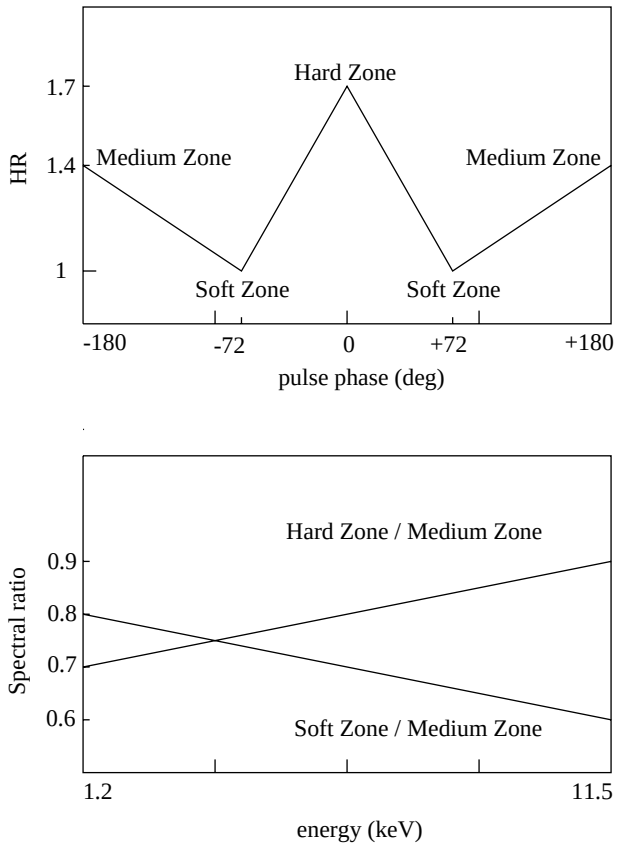

Fig. 5. – Hardness ratio and pulse-phase spectroscopy for the toy model of sect. **4**.

region. The pulse profile produced by the spin of the NS can then be calculated for particular values of the observer inclination angle (i), and the co-latitude of the magnetic axis with respect to the spin axis (m). The emission region is divided into a number of "bricks" (fig. 1), each of which is small enough such that its surface presents a single angle to the line of sight. With a suitable transformation matrix it is possible to determine which bricks are visible for a given i and m, *i.e.* unobscured by the body of the NS, at any particular spin phase. The emission process considered is thermal bremsstrahlung, Thomson scattering is also considered: given the light path (d) over which a particular brick is seen, the optical depth (τ) is $\int_0^d \rho\sigma_{\mathrm{T}}/m_{\mathrm{p}}\,\mathrm{d}x$, where ρ is the density, m_{p} the proton mass and σ_{T} the Thomson cross-section. The assumption of optically thin bremsstrahlung is valid providing that the solid angle over which $\tau \gg 0$ is $\ll 4\pi$. This condition is satisfied in the case of a thin-walled, hollow cone as $\tau \ll 1$ except over the small phase interval when the observer looks directly down the cone walls. If a blackbody-like region is present at the base of the cone in a short ring or slab, its contribution is also computed; for this region the occultation effects of the NS body could be very important. It is possible to produce pulse profiles in the hard and soft spectral regimes and the relative hardness ratio curve (HR), depending on the temperature profile.

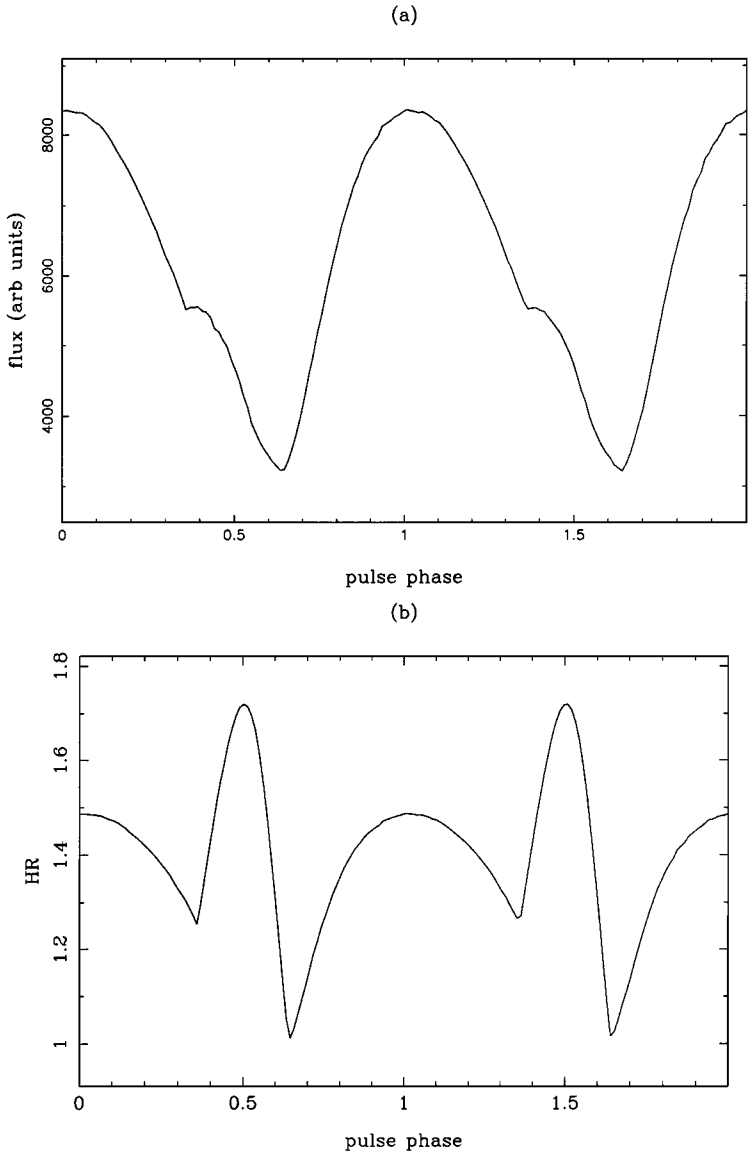

Fig. 6. – Upper panel: simulated light curve. Lower panel: simulated hardness ratio.

4. – Application to X Persei

As an example we try to reproduce the pulse profile of the X-ray source X-Persei observed by the *Ginga* satellite. This source is particularly interesting because of the very complex phase-modulated HR. The spectrum of this source is consistent with thermal bremsstrahlung at a temperature of 7–12 keV (Becker *et al.* 1979, White *et al.* 1976, White *et al.* 1982), or a power law resulting from subsequent Comptonization (Sunyaev and Titarchuk 1980) as reported by Murakami *et al.* (1987) and Robba and Warwick (1989). The light curve, the HR and the pulse-phase spectroscopy from the *Ginga* data are shown

TABLE I. – *Variation of the visible flux from different cone regions with spin phase.*

ϕ (degrees)	Cone section			BR
	top	middle	bottom	
0	100%	100%	0%	100%
72	100%	100%	33%	0%
180	100%	100%	100%	0%

in figs. 2 and 3 (Robba *et al.* 1996). Fan beam bremsstrahlung emission plus a blackbody-like region near the NS crust can explain the general shape of the pulse profile and the main features of the hardness ratio and the pulse-phase spectroscopy. As conceptual aid we present a toy model of the cone and the blackbody-like region (BR) in fig. 4, the emissivity and the hard/soft fraction for various zones of the cone and the BR are also displayed. We assume that $i \simeq m$, to allow the line of sight to pass close by the magnetic axis, and choose the phase angle (ϕ) in such a way that $\phi = 0$ corresponds to looking along the magnetic axis. Table I shows the visible flux from different cone regions at a number of spin phases, as a percentage of the total flux from the region considered. While the top and middle regions of the cone are always visible, the fan emission nature of the bremsstrahlung component means that the emission from the bottom region of the cone is negligible when the observer's line of sight is aligned along the magnetic axis, but is only partially shaded at intermediate angles. The BR is mostly visible only when the the line of sight is close to the magnetic axis, due to the combined effect of the large opening angle of the cone, the variation in the magnetic field strength over the cone walls and the absorption due to the cone walls (Robba *et al.* 1996). In table II the resulting intensity of the hard and soft bands are shown, together with the HR for different spin phases, and the results of phase spectroscopy. In fig. 5 the HR and the phase spectroscopy are schematically sketched, from which it is possible to see that this toy model explains the main features of the HR and of the phase spectroscopy.

The results of a full numerical simulation of the X Persei light curve and HR, using the method outlined in sect. 3, are presented in fig. 6. Here a linear gradient is adopted for the

TABLE II. – *Flux* (*arbitrary units*) *and Hardness Ratio for different phases. Spectral ratios between the Hard Zone* (H)*, the Medium Zone* (M)*, and the Soft Zone* (S) *as defined in* fig. 5.

ϕ (degrees)	status	soft				hard				HR
		top	middle	bottom	BR	top	middle	bottom	BR	(hard/soft)
		3	4	0	0	1	4	0	7	
0	H	7				12				1.7
		3	4	1	0	1	4	3	0	
72	S	8				8				1.0
		3	4	3	0	1	4	9	0	
180	M	10				14				1.4
phase	H/M	0.7				0.9				
spec.	S/M	0.8				0.6				

density and temperature profiles along the cone walls, with $T_{\rm top} = 10\,{\rm keV}$, $T_{\rm bot} = 3\,{\rm keV}$, $\rho_{\rm top} = 0.1\rho_{\rm bot}$, cone opening half-angle $= 30°$, angular wall width $= 9°$, $i = 40°$, $m = 30°$, and a cone height of $5R_{\rm NS}$. Comparison with fig. 2 shows the simulation results to be in good agreement with the observational data.

REFERENCES

ARONS J. and LEA S. M., *Astrophys. J.*, **235** (1980) 1016.
BASKO M. M. and SUNYAEV R. A., *Astron. Astrophys.*, **42** (1975) 311.
BECKER R. H. *et al.*, *Astrophys. J. Lett.*, **227** (1979) L21.
LAMB F. K. *et al.*, *Astrophys. J.*, **184** (1973) 271.
MESZAROS P., HARDING A. K., KIRK J. G. and GALLOWAY D. J., *Astrophys. J. Lett.*, **266** (1983) L33.
MURAKAMI T. *et al.*, *Publ. Astron. Soc. Jpn.*, **39** (1987) 253.
ROBBA N. R. and WARWICK R. S., *Astrophys. J.*, **346** (1989) 469.
ROBBA N. R. *et al.*, *Astrophys. J.*, **472** (1996) 341.
SUNYAEV R. A. and TITARCHUK L. G., *Astron. Astrophys.*, **86** (1980) 121.
WANG Y.-M. and FRANK J., *Astron. Astrophys.*, **93** (1981) 255.
WANG Y.-M. and WELTER G. L., *Astron. Astrophys.*, **113** (1982) 113.
WHITE N. E. *et al.*, *Mon. Not. R. Astron. Soc.*, **176** (1976) 201.
WHITE N. E. *et al.*, *Astrophys. J.*, **263** (1982) 277.
WHITE N. E. *et al.*, *Astrophys. J.*, **270** (1983) 711.